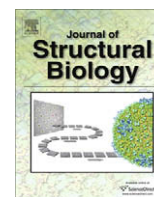




Contents lists available at ScienceDirect

## Journal of Structural Biology

journal homepage: [www.elsevier.com/locate/yjsbi](http://www.elsevier.com/locate/yjsbi)

## Transversely isotropic distribution of sulfated glycosaminoglycans in human medial collateral ligament: A quantitative analysis

Heath B. Henninger<sup>a,b</sup>, Steve A. Maas<sup>a,b</sup>, Jonathan H. Shepherd<sup>a</sup>, Sarang Joshi<sup>a,b</sup>, Jeffrey A. Weiss<sup>a,b,c,\*</sup>

<sup>a</sup> Department of Bioengineering, University of Utah, 50 South Central Campus Drive, Room 2480, Salt Lake City, UT 84112, USA

<sup>b</sup> Scientific Computing and Imaging Institute, University of Utah, 72 South Central Campus Drive, Room 3750, Salt Lake City, UT 84112, USA

<sup>c</sup> Department of Orthopaedics, University of Utah, 30 North 1900 East, Room 3B165, Salt Lake City, UT 84132, USA

## ARTICLE INFO

## Article history:

Received 5 August 2008

Received in revised form 17 November 2008

Accepted 26 November 2008

Available online 24 December 2008

## Keywords:

Ligament

Glycosaminoglycan

Dermatan sulfate

Transverse isotropy

Image analysis

## ABSTRACT

Decorin and its associated glycosaminoglycan (GAG) side chain, dermatan sulfate (DS), play diverse roles in soft tissue formation and potentially aid in the mechanical integrity of the tissue. Deeper understanding of the distribution and orientation of the GAGs on a microscopic level may help elucidate the structure/function relationship of these important molecules. The hypothesis of the present study was that sulfated GAGs are aligned with transversely isotropic material symmetry in human medial collateral ligament (MCL) with the collagen acting as the axis of symmetry. To test the hypothesis, sulfated GAGs were visualized using transmission electron microscopy (TEM). Three orthogonal anatomical planes were examined to evaluate GAG distributions against symmetry criteria. GAG populations were differentiated using targeted enzyme digestion. Results suggest that sulfated GAGs including DS, chondroitin sulfates A and C, as well as other sub-populations assume transversely isotropic distributions in human MCL. Sulfated GAGs in the plane normal to the collagen axis were found to be isotropic with no preferred orientation. GAGs in the two planes along the collagen axis did not statistically differ and exhibited apparent bimodal distributions, favoring orthogonal distributions with over half at other angles with respect to collagen. A previously developed model, GAGSim3D, was used to interpret potential TEM artifacts. The data collected herein provide refined inputs to micro-scale models of the structure/function relationship of sulfated GAGs in soft tissues.

© 2008 Elsevier Inc. All rights reserved.

### 1. Introduction

Ligaments are passive collagen based tissues that stabilize articulating joints by connecting bone to bone. Ligament is hierarchically organized and contains approximately 70% Type I collagen by dry weight (Amiel et al., 1990; Kastelic et al., 1978; Ottani et al., 2001). The balance of the hydrated tissue consists of “ground substance” which is a gel-like mixture of proteins, proteoglycans (PGs), glycosaminoglycans (GAGs), and water surrounding the ordered collagen fibrils. GAGs in ligament constitute 0.2–5.0% of the total dry weight (Amiel et al., 1984; Gillard et al., 1977). Understanding the distribution and structural organization of GAGs in ligament may shed light on their role in connective tissues.

The decorin PG is the most prevalent PG in ligaments in terms of molar quantity (Ilic et al., 2005) and has been shown to play diverse roles in connective tissues from regulation of collagen fibril formation (Vogel et al., 1984) to influencing the mechanical prop-

erties of the tissue (Danielson et al., 1997; Robinson et al., 2005). Decorin localizes to the surface of collagen fibrils in a repeating fashion (Pringle and Dodd, 1990) and is thought to bind every 67 nm at the D-period band gap in the tropocollagen quarter-stagger pattern (Scott, 1996; Scott and Orford, 1981; Scott et al., 2004). The exact 3D conformation of decorin, including whether it functions as a monomer or dimer, remains a subject of debate (Goldoni et al., 2004; Scott, 2003; Scott et al., 2004; Weber et al., 1996).

The decorin core protein is covalently bound to either a single dermatan sulfate (DS) or a single chondroitin sulfate (CS) GAG side chain near the amino terminus (Chopra et al., 1985). Flexibility within the iduronate residues along the DS backbone may allow the GAG many possible conformations with respect to the collagen fibril (Scott, 1992; Venkataraman et al., 1994). DS chains can self-associate under physiological conditions, containing up to ten or more individual GAG chains as an aggregate (Ernst et al., 1995; Scott, 1992). The biglycan PG, although significantly less prevalent than decorin in ligament (Ilic et al., 2005), contains two DS and/or CS side chains (Trowbridge and Gallo, 2002).

The GAG side chain of decorin has been described as contributing to the mechanical integrity of the host tissue by forming aggregate interfibrillar bridges between adjacent collagen fibrils (Liu

\* Corresponding author. Address: Department of Bioengineering, University of Utah, 50 South Central Campus Dr., Room 2480, Salt Lake City, UT 84112, USA. Fax: +1 801 585 5361.

E-mail address: [jeff.weiss@utah.edu](mailto:jeff.weiss@utah.edu) (J.A. Weiss).

et al., 2005; Redaelli et al., 2003; Scott, 2001; Scott and Thomlinson, 1998; Vesentini et al., 2005). Recent experiments examined ligament's continuum level response to quasi-static shear and tensile deformation using an enzyme degradation method and found no macroscopic contribution provided by DS or CS GAGs (Lujan et al., 2007). GAGs may contribute to the microscopic mechanical environment but experimental validation on native tissues is extremely difficult. GAG chains may also act to lubricate the interfibrillar space (Scott, 2003) and support compressive loads via water retention, similar to larger PG/GAG aggregates like aggrecan and versican in cartilage (Basalo et al., 2005, 2007, 2004).

The material symmetry of ligament in relation to its mechanical properties is often described as transversely isotropic on the macroscopic scale (Gardiner and Weiss, 2003; Quapp and Weiss, 1998; Weiss and Gardiner, 2001; Weiss et al., 2002; Yamamoto et al., 2000). Materials exhibiting transverse isotropy consist of a single preferred axis of symmetry. The plane normal to the preferred axis is isotropic, meaning it has the same construction, constituents, and material properties when tested in any direction on that plane. Consequently, any two sections taken along the preferred axis (orthogonal to the isotropic plane) will share the same properties as one another but may differ from the isotropic plane. In ligament, fibrillar Type I collagen represents the axis of symmetry and the ground substance an isotropic bulk material surrounding the collagen. Quantification of material symmetries of the constituents within the ground substance is lacking in the literature.

Characterization of micro-scale GAG symmetries is critical for formulation of molecular models that attempt to describe the mechanical environment within biological tissues. Previous research on GAGs in cartilage modeled the initial GAG distribution as stochastic. When loaded, GAGs assumed anisotropic symmetries, favoring orientations perpendicular to the applied loads (Quinn et al., 2001). This anisotropy was linked to changes in the permeability of the cartilage, suggesting that GAG orientation influences both the global and micro-scale viscoelastic response of the tissue.

Redaelli et al. performed a computational analysis of micro-scale GAG force transfer in tendon (Redaelli et al., 2003). The study recognized that the assumption of an orthogonal GAG population may generate misleading results. Should a significant percentage of GAGs not assume perfectly orthogonal orientations, the contribution of each GAG to the overall force transfer would be a function of the relative orientation with respect to the adjacent collagen fibrils. Clearly a better understanding of GAG distribution and symmetry would lead to a more refined interpretation of GAG contributions to overall tissue function.

The hypothesis of this study was that sulfated GAGs assume a transversely isotropic distribution about the local collagen axis in human medial collateral ligament (MCL). The objective was to measure GAG orientation in three orthogonal anatomical planes using transmission electron microscopy (TEM) and image processing techniques. Enzymatic degradation with chondroitinase B was used to differentiate between populations of sulfated GAGs.

## 2. Methods

### 2.1. Tissue sample selection

Ten unpaired human knees were obtained from 10 separate male donors (age 47–65, median 54). Specimens remained frozen until the time of dissection and were allowed to thaw before being dissected free of fat and extraneous soft tissue. Knees with surgical scars, ligament injury or cartilage degeneration characteristic of osteoarthritis were eliminated. The medial collateral ligament (MCL) was removed at both the femoral and tibial insertion sites

and fine dissected to remove any overlying fascia. The ligaments were kept hydrated with normal saline during tissue isolation. Bulk tissue was trimmed to remove a sample from the mid-substance of each MCL. Each sample was then halved to obtain paired specimens.

### 2.2. Glycosaminoglycan digestion

In order to investigate the distribution of DS versus other sulfated GAGs, enzymatic treatment with chondroitinase B (ChB) was performed on one of the two samples (randomly chosen) from each MCL while the other sample was used as control. ChB specifically degrades DS (Ernst et al., 1995). This procedure was identical to that used in previous studies (Henninger et al., 2007; Lujan et al., 2007). Briefly, all samples were soaked for 1 h in buffer (15 ml of 20 mM Tris pH 7.5, 150 mM NaCl, 5 mM CaCl<sub>2</sub>) at room temperature with protease inhibitors (1 tablet of mini-complete per 10 ml buffer). Samples were then bathed for an additional 6 h in buffer or buffer + 1.0 U/ml ChB. Pilot worked showed 0.25 U/ml 6 h completely degraded all DS (data not shown). After treatment, samples were placed in a stop buffer (15 ml of 20 mM Tris pH 7.5, 150 mM NaCl, 10 mM EDTA) to halt further chondroitinase activity. To obtain sufficient enzyme for use in this study, ChB was cloned in *Flavobacterium heparinum* as previously described (Pojasek et al., 2001). Chondroitinase B specificity was tested using the previous protocols (Henninger et al., 2007; Lujan et al., 2007).

### 2.3. Transmission electron microscopy

Frozen specimens were sectioned along three orthogonal planes corresponding to anatomical directions with respect to the local collagen fiber orientation (Fig. 1). Both the Anterior–Posterior (AP, sagittal) and Medial–Lateral (ML, coronal) planes were aligned along the collagen axis while the transverse (T) plane viewed the collagen in cross-section. Twenty micron sections from each plane of the specimen were obtained on a cryostat (Leica CM3050S, Exton PA) at –25 °C. Sections were then prepared for TEM visualization using previously reported methods (Henninger et al., 2007;

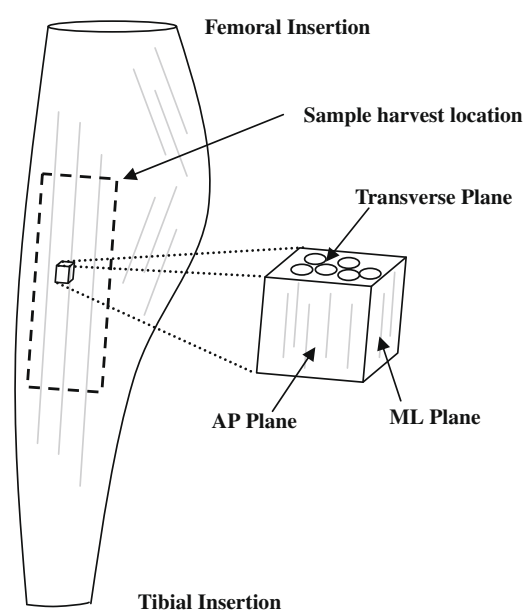


**Fig. 1.** Schematic of sample harvest in the medial collateral ligament. Specimens were isolated from the mid-substance of the MCL. The three anatomical planes were sectioned with respect to the local collagen orientation. (AP = sagittal plane, ML = coronal plane).

Lujan et al., 2007). Sulfated GAGs were targeted using an electron dense stain at critical electrolyte concentration for 3 h at 37 °C (0.05% Cupromeronic Blue (Sigma, St. Louis, MO), 2.5% glutaraldehyde, 25 mM sodium acetate, 0.1 M MgCl<sub>2</sub>, pH 5.8) (Cribb and Scott, 1995; Haigh and Scott, 1986). Digital images were collected on a Hitachi H7100 TEM with a tungsten filament. A minimum of ten digital images were captured from different areas of a section so average GAG distributions could be obtained.

#### 2.4. Improved image processing algorithm

Previous work described an image processing algorithm that isolated stained GAGs from a grayscale TEM image (Henninger et al., 2007). The algorithm was streamlined for the present research to improve sensitivity of GAG detection, calibration of grayscale thresholding, and processing speed. The improved algorithm was developed in Matlab using the Image Processing Toolbox (Mathworks, Natick, MA). The Matlab input file is available for download as Supplementary Material on the Journal web page.

The collagen fibril axis was obtained from TEM images by interactively digitizing four vectors along the predominant fibril axis using ImageJ (National Institutes of Health). The average angle of the collagen fibrils with respect to the horizontal was saved to a data file.

The improved algorithm reduced the image analysis to three basic steps (Fig. 2). First, images were treated with a local equalization filter to rescale the grayscale histograms. Equalization significantly simplified the process of identifying image-specific grayscale threshold values. The equalization filter had the added

benefit of retaining GAG continuity against the background noise (Fig. 2B). Next, a median filter was applied to further reduce background noise while improving GAG homogeneity (Fig. 2C).

Images were converted to binary and isolated GAGs were reduced to wire frame elements using a skeletonization function (Fig. 2D). Since visualized GAGs are likely aggregates of smaller GAG chains (Ernst et al., 1995; Scott, 1992) branches are either GAGs projecting off the predominant chain or two or more GAGs overlapping through the thickness of the specimen. Two dimensional TEM images could not discern between these branching modes, thus only the longest chain of connected pixels was retained to represent the GAG. Finally, a size filter was applied to remove objects below 10 pixels in length since they were residual noise artifacts or GAGs exiting the viewing plane directly. Small objects were subject to extreme error in orientation processing and thus eliminated from all images.

Once wire frame elements were isolated a principal component analysis (PCA) was performed on the pixel coordinates (Duda et al., 2001). This yielded a covariance matrix that was transformed into the eigenvectors of the GAG. Taking the maximum eigenvector of each object as its orientation, a unique angle was quantified with respect to the collagen fibril axis.

#### 2.5. Continuous GAG distributions

In order to compare GAG orientation from various planes and treatment cases, angle measures were compiled into continuous distributions. Orientation was measured from 0° to 180° with respect to the collagen axis. Since it was unclear which end(s) of

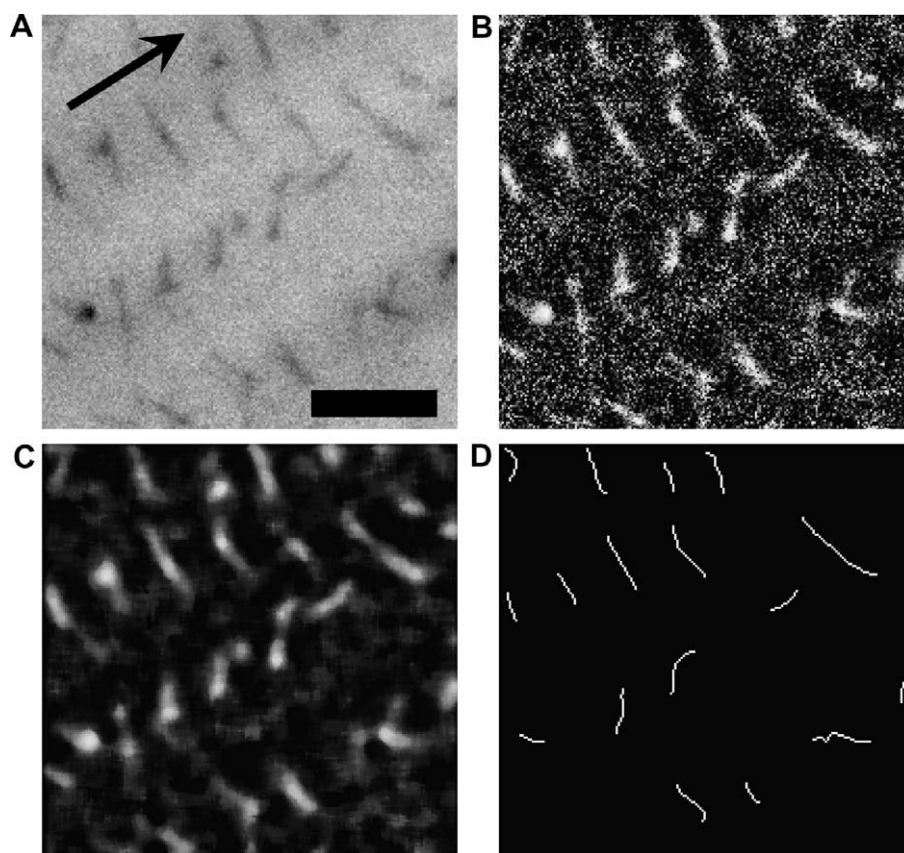


**Fig. 2.** Demonstration of the improved image processing algorithm used to isolate sulfated GAGs in TEM images. Panel A, portion of sample image with sulfated GAGs stained against a grayscale collagen background (arrow denotes collagen axis). Panel B, local grayscale equalization filtering. Panel C, median filtering of equalized image. Panel D, wire frame representation used to calculate orientation of stained GAGs. Branched wire frame objects were broken and only the longest continuous chain was retained. Size filtering was applied to remove detected GAGs below a critical length (10 pixels). Bar = 50 nm.

the GAGs were associated with adjacent collagen fibrils, the angle measure was reflected into the 0° (coaxial to collagen) to 90° (orthogonal to collagen) range to simplify interpretation.

Continuous distributions were generated using a Parzen windowing technique (Duda et al., 2001). Unit Gaussian curves were assigned for each detected GAG and summed, where angle with respect to collagen represented the mean, and variance was a function of the GAG's shape. Molecular contour varies in two dimensional TEM due to 2D projection artifacts and GAG overlap through the specimen thickness (Henninger et al., 2007; Van Kuppevelt et al., 1987). Nearly linear GAGs contain little variance perpendicular to their length and result in robust measures of orientation due to minimized covariance with respect to the image space. Amorphous GAGs contain higher degrees of covariance and in turn less confident assignment of primary axes.

Variance of the GAG was defined as the ratio of the minimum to the maximum eigenvalue as determined by PCA. The ratio of eigenvalues yielded a molecular aspect ratio where values close to one (1) suggest a highly amorphous GAG (Fig. 3, right) and values close to zero (0) indicate highly linear GAGs (Fig. 3, left). When summed, unit Gaussians from two GAGs with the same perceived angle, but different shape, scale to weight the linear GAG more than the amorphous GAG (Fig. 3). In practice all variances were less than one and caused considerably noisy distributions. To alleviate this issue, a static multiplier was included to scale up variances such that fine detail of the distribution was not lost but the overall curve was devoid of dramatic point to point noise.

The multiplier was refined manually. Perfectly straight GAGs had an eigenvector ratio of zero. These generated a Dirac Delta function at the determined angle. In this case variance was set to 0.1 so a Gaussian distribution could be defined explicitly. Straight GAGs therefore highly influenced the overall distribution since they were heavily weighted due to the small variance. Otherwise

the multiplier was set to 1000. Most detected GAGs had some degree of curvature and their variances ranged from 0.1 to 1. The value 1000 was determined manually to provide sufficient resolution in a set of test images such that the angle distribution retained the shape of one with an extreme variance multiplier (10,000 = over-smoothed) but was reactive to populations of highly linear GAGs.

GAG orientation distributions were generated for each image, plane of section, treatment case, and knee and discretized into 1° increments to simplify comparison and data handling. Angle distributions from each image in a plane/treatment/sample group were averaged to generate a representative distribution for that group. A total of 500 summed distributions were generated from 500 TEM images.

## 2.6. Transverse isotropy criteria

Transversely isotropic material symmetry is defined by an axis normal to a plane of isotropy about which any number of planes can be sectioned that share the same material properties and composition. The primary axis in this study was the local collagen direction in the ligament. To be considered transversely isotropic, sulfated GAG distributions in planes along the collagen axis (AP, ML) could not significantly differ from one another and the plane normal to the collagen axis (T) was required to have an isotropic GAG distribution.

## 2.7. Statistical analysis

Results from TEM images were analyzed with the independent *t*-test to assess differences in the number of detected GAGs between control and ChB treated images. Both ANOVA with Tukey post hoc and independent *t*-tests were used to examine differences in median GAG angle for control versus ChB treatment as well as plane versus plane within each treatment group. The non-parametric Kolmogorov–Smirnov (KS) test was used to compare GAG distributions between control and ChB treated cases as well as between planes within each treatment group. Significance for all tests was set at  $\alpha = 0.05$ .

## 3. Results

### 3.1. GAG detection and efficacy of ChB

The total number of sulfated GAGs detected (by number) in both control and treated samples was in good agreement with published data (Henninger et al., 2007). The mean number of GAGs in the control AP plane was  $363.5 \pm 83.4$ , while in the ChB treated AP plane  $35.1 \pm 30.5$  (88.2  $\pm$  12.7% reduction). Mean GAG counts for the control and ChB treated ML plane were  $395.4 \pm 113.1$  and  $45.5 \pm 26.5$ , respectively (87.1  $\pm$  9.5% reduction). The control and ChB treated GAG counts for the transverse plane were  $255.3 \pm 68.8$  and  $49.5 \pm 30.7$ , respectively, resulting in a  $76.9 \pm 18.9\%$  reduction in sulfated GAGs. Sulfated GAG count in control images was significantly different than ChB treated in all three planes (all  $p \approx 0.000$ ). The AP and ML planes did not significantly differ in either the control ( $p = 0.887$ ) or ChB treated cases ( $p = 0.835$ ). The transverse plane had a significantly different control GAG count than either the AP or ML planes (all  $p < 0.032$ ), but did not differ from either with respect to ChB treated images (all  $p > 0.688$ ).

### 3.2. Orientation of sulfated GAGs

In both the AP and ML planes the control GAG distribution assumed an inverse Gaussian profile with maxima near coaxial and orthogonal orientations with respect to the collagen axis (Fig. 4).

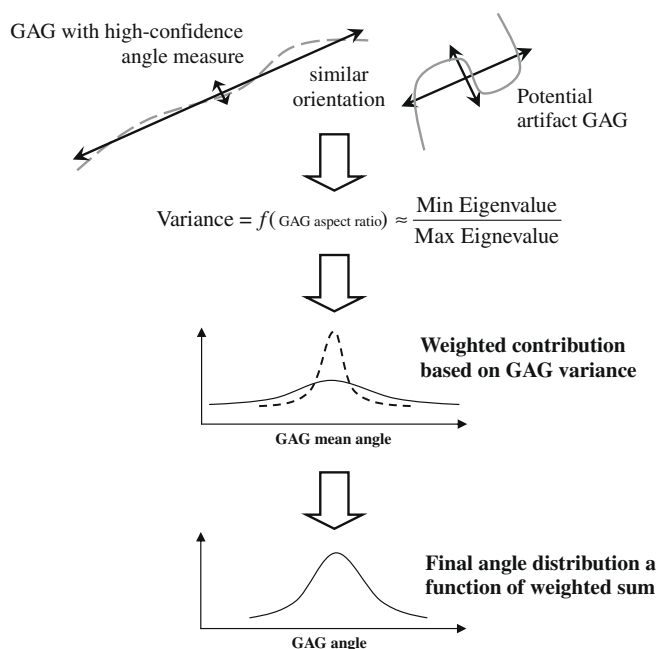


**Fig. 3.** Weighting of GAG orientation as a function of wire frame shape. Each GAG contributes to the overall angle distribution individually with a unit Gaussian curve defined by the angle of the maximum eigendirection (mean) and ratio of eigenvalues associated with its shape (variance). The GAGs shown would both contribute at the same mean angle. The GAG on the left (dashed line) is highly linear and therefore yields a smaller variance and stronger weight than the irregular GAG shown on the right (solid line). The cumulative angle distribution is a function of the weighted curves with high-confidence GAGs influencing the overall distribution more than low-confidence GAGs.

GAGs remaining after ChB treatment were skewed toward coaxial distributions. The transverse plane displayed a relatively flat distribution across all angles for both the control and ChB treatment cases. Note that “inverse Gaussian” is not defined over a semi-infinite domain but in this case is used to describe symmetry about a mean/median angle.

Comparing treatment cases by plane showed significantly different median angles. Both the AP and ML planes showed a significant decrease in median angle with ChB treatment ( $39.9 \pm 7.4^\circ$  to  $29.9 \pm 1.2^\circ$  for AP,  $40.3 \pm 5.4^\circ$  to  $34.0 \pm 2.9^\circ$  for ML, both  $p < 0.012$ ) as can be seen in the profile shift from the inverse Gaussian to coaxially skewed distributions (Fig. 4, left and center panes). The transverse plane also showed a significant change ( $38.7 \pm 2.5^\circ$  to  $41.0 \pm 0.5^\circ$ ,  $p = 0.024$ ), although ChB treatment caused a slight increase in median angle. Significance was detected due to extremely small variances associated with the measurements.

When comparing control distributions by plane, there were no significant differences in median angles (all  $p > 0.829$ ). ChB treated distributions yielded significant differences between each plane (all  $p \approx 0.000$ ).

In order to illustrate the differences in distribution shape using the Kolmogorov–Smirnov (KS) test, the profiles were normalized (Fig. 5). An additional set of distributions were generated to represent the DS population. Since ChB selectively degrades DS (Ernst et al., 1995) the DS population was derived as the difference between control and ChB treated profiles. It is clear in Fig. 5 that the AP and ML planes are qualitatively similar and appear to vary from the transverse plane. Note that median angle statistics were not derived for the DS populations since their profiles were a difference between two generated profiles and thus no raw data existed.

As expected from qualitative examination of Fig. 4, the control distributions for AP and ML planes did not appear to be derived from the same population distribution as their ChB treated counterparts (both  $KS \geq 0.600$ , both  $p \approx 0.000$ ). On the contrary, the shape of the control and ChB treated distributions in the transverse plane did not reject the null hypothesis that they are derived from the same population distribution ( $KS = 0.133$ ,  $p = 0.376$ ).

The shape of the AP plane did not significantly vary from the ML in the control or DS distributions (both  $KS \geq 0.144$ , both  $p \geq 0.104$ ) but did in the ChB treated case ( $KS = 0.233$ ,  $p = 0.012$ ). Qualitatively the ChB treated distributions are quite similar (Fig. 5, center pane) but the KS test is a function of the cumulative distribution. Small deviations in magnitude of the curves provide enough difference for the highly sensitive KS test to detect a significant difference.

The transverse plane differed significantly from the AP and ML planes in control ( $KS \geq 0.256$ ), ChB treated ( $KS \geq 0.600$ ), and DS cases ( $KS \geq 0.222$ ) (all  $p < 0.020$ ) (Fig. 5). The transverse distributions appear quite flat in comparison to the contoured AP and ML distributions for each treatment case examined.

### 3.3. Improved image analysis

The improved image processing algorithm significantly reduced execution time by over 80% from approximately 3 min down to 30 s per image. Alterations in algorithm execution speed coupled with the streamlined process flow significantly reduced grayscale threshold calibration times to the range of 1–3 min per image. Homogeneity of images after grayscale equalization allowed batches of images from the same TEM grid to share calibration values, again significantly reducing the amount of user interaction and time required to optimize the image parameters. Detection of sulfated GAGs against the collagen background did not significantly differ from the previous algorithm. Error in GAG detection, either by false detection or omission, was near 5% of the total GAGs detected per image. Direct comparison of a finite set of images using the original and modified algorithms found no differences in shape or magnitude of the derived orientation distributions.

## 4. Discussion

The results of this study support the hypothesis that sulfated GAGs are distributed with transversely isotropic symmetry in the human MCL. First, GAGs have an isotropic material symmetry in the plane normal to the collagen axis. Note that in the transverse plane the angle measured is merely a reference since the collagen axis is exiting the plane of view. Fig. 4 (right pane) shows both the control and ChB treated populations in the transverse plane have an approximately equal probability of being found in any orientation measured. Consequently, the DS population derived from the control and ChB profiles also exhibits an equal probability of finding GAGs in any orientation. These distributions therefore satisfy the criteria of the isotropic normal plane.

The second criteria of a transversely isotropic material symmetry is that any two planes that are coaxial to the preferred axis and normal to the isotropic plane must not differ significantly in their respective GAG distributions. Both the AP and ML planes display qualitatively similar distributions for control, ChB treated, and DS populations (Figs. 4 and 5), and both are coaxial to the collagen and normal to the transverse plane. Statistically, it can be said that AP/ML control and DS distributions did not arise from dissimilar

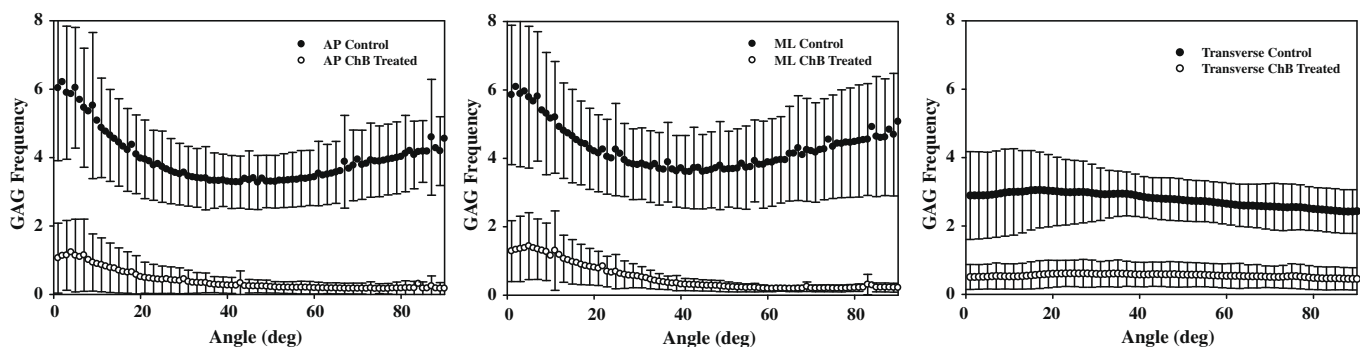


**Fig. 4.** Distribution of sulfated GAGs with respect to the local collagen fibril orientation. Left Pane, GAG distribution in the AP plane. GAGs in control images had a median angle of  $39.88^\circ$ . After treatment with ChB sulfated GAGs were skewed toward coaxial distributions with a median angle of  $29.85^\circ$ . Middle Pane, GAG distribution in the ML plane. Control and treated cases were similar to those in the AP plane with median sulfated GAG angles in control and treated of  $40.25^\circ$  and  $34.01^\circ$ , respectively. Right Pane, GAG distribution in the plane transverse to the collagen fibrils. Both the control and ChB treated distributions were nearly flat with median GAG angles of  $38.67^\circ$  and  $40.96^\circ$ , respectively. GAG reduction between control and ChB treated cases was significant in each plane (all  $p \approx 0.000$ ) and ranged from 80.6% to 90.3%.

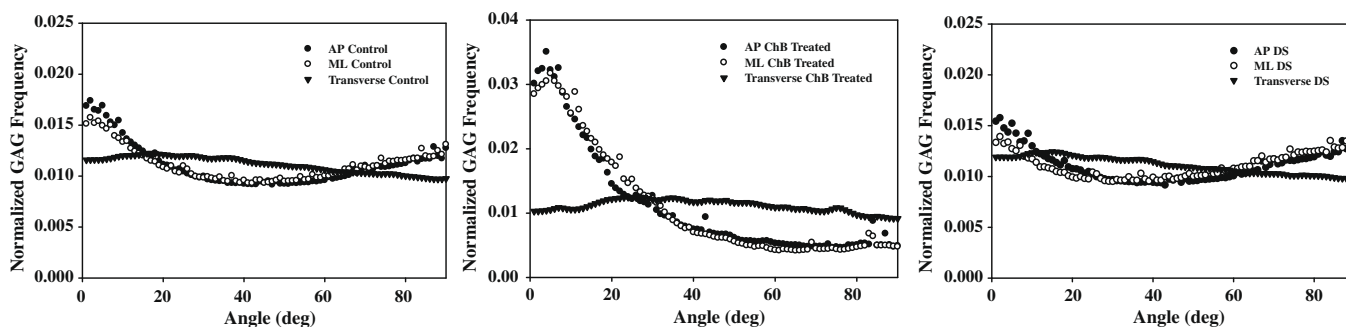


**Fig. 5.** Comparison of normalized sulfated GAG distributions between planes by treatment case. Left Pane, Control GAG distribution by plane. Note the good agreement of AP and ML planes across the range of angles. Middle Pane, ChB treated GAG distribution by plane. Again there is good agreement between AP and ML planes. Right Pane, DS GAG distribution by plane. Profiles were derived from the difference between Control and ChB treated curves. As with both Control and ChB panes, the AP and ML planes show good agreement while the transverse plane is relatively flat.

populations as the null hypothesis of the KS test was not rejected. On the contrary, ChB treated distributions of the AP/ML planes rejected the null hypothesis of the KS test due to minor differences in magnitude at the origin of the curves. Since the KS is a non-parametric test it is based on a summed rank of the cumulative distribution function of each curve. This makes the KS test sensitive to small deviations in magnitude that, when compiled, exceed the significance level in the ChB treated profiles. Understanding this limitation, qualitative inspection of the ChB treated profiles of the ChB treated AP and ML planes shows that they are nearly identical in shape and magnitude and in the scope of this work are essentially the same.

These data support that as a population sulfated GAGs are transversely isotropic, but underlying populations can be isolated using enzymatic digestion. Removal of approximately 85% of sulfated GAGs with ChB is in agreement with previous studies stating that DS is the predominant sulfated GAG in ligament (Henninger et al., 2007; Ilic et al., 2005; Iozzo, 1999). Per the criteria above, the subpopulation of DS also displays transverse isotropy.

Sulfated GAGs remaining after ChB treatment are likely chondroitin sulfates A and C (Cs-4, Cs-6), keratan, or heparan sulfates (Amiel et al., 1990; Gillard et al., 1977; Iozzo, 1998; Scott, 1985; Vogel et al., 1993). Pilot work done with chondroitinase ABC (data not shown), which degrades CsA, CsC, and DS, demonstrated that over 98% of sulfated GAGs were removed from TEM images of treated ligament. This supports that the majority of GAGs remaining after ChB treatment are CsA and CsC. It can then be inferred that CsA and CsC as a population are also transversely isotropic about the collagen axis.

The GAG distributions presented in this study must be interpreted with caution since artifacts arise when measuring orienta-

tion of two dimensional data from a three dimensional population (Henninger et al., 2007; Van Kuppevelt et al., 1987). Projection and clipping artifacts lead to the loss of information about the true 3D population underlying the 2D population measured in TEM. As this was a comparative study, any artifacts arising in a given image should be found in any other image. All comparisons were made on images processed with the same algorithms and therefore relative errors between data sets should be negated.

Henninger et al. described a technique to three dimensionally model an idealized GAG population that may be used to interpret the two dimensional results collected from TEM (Henninger et al., 2007). The model, GAGSim3D, was updated for this study to include the ability to simulate all three anatomical planes (GAGSim3D update also available on the Journal web page). Results of 10 models (30 sections, 3 planes per model) were compared and found to have satisfied the criteria of transverse isotropy as described in the present methods. Direct comparison to the 2D TEM yielded an interesting artifact not detected in the previous study (Fig. 6).

GAGs detected in the transverse plane (Fig. 6, Right pane) show good agreement between the TEM and GAGSim3D data, yielding an isotropic GAG distribution. Profiles of the AP and ML planes differ between TEM and the model (Fig. 6, Left and Middle panes). This is not an artifact of the new algorithm as direct comparison of the new and old algorithms were nearly identical in magnitude and shape. GAGSim3D data was also compared using both sets of image analysis software and again, no significant differences were found in the shape of the profiles in any plane. The difference arises from two sources. First, the new data set likely included a higher percentage of truly coaxial DS GAGs than the previous study. The second source is the model's inability to truly recreate coaxial GAGs. Modeled GAGs were constrained so they originated from

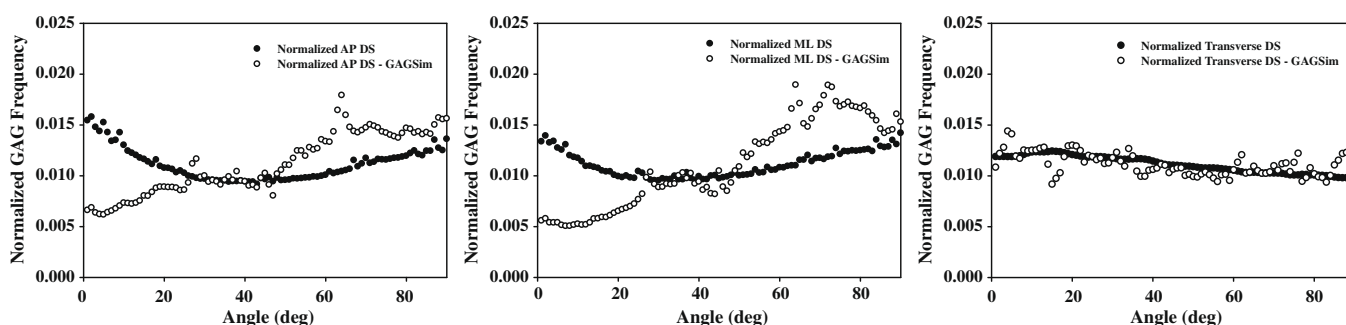


**Fig. 6.** Comparison of normalized DS GAG distributions between TEM and GAGSim3D by plane. Left Pane, DS in AP plane. Middle Pane, DS in ML plane. Disagreement in AP and ML planes between TEM and GAGSim3D arises from sensitivity of the algorithm to subtleties in grayscale intensity, limitation of the model to produce coaxial GAGs, increased incidence of coaxial GAGs in the data, and normalization of the data. Right Pane, DS detected in transverse plane is in good agreement between TEM and GAGSim3D.

one collagen fibril and terminated to a different collagen fibril in an attempt to model interfibrillar bridging. This prevented GAGs from associating along a single collagen and assuming perfectly coaxial orientations. GAGs detected in the coaxial range (0–30°) of the model were therefore projecting into the viewing plane in 3D space. This population, when projected into 2D, appeared coaxial but was lacking truly coaxial GAGs to inflate the population. When normalized for comparison between TEM and GAGSim3D the relative populations appear to arise from different populations. Isolating only GAGs from 40–90°, normalization yielded very similar population distributions. GAGs in the transverse plane are not subject to this interpretation error since none are viewed directly along the collagen axis in this perspective. Accounting for this artifact, one can clearly see that both TEM and GAGSim3D data support transversely isotropic material symmetry.

Sulfated GAGs have been suggested to bridge adjacent collagen fibrils and transmit forces between fibrils (Redaelli et al., 2003; Scott, 2003; Scott and Thomlinson, 1998; Vesentini et al., 2005). Other studies have qualitatively described the GAG distribution as generally orthogonal to collagen with some percentage of GAGs not falling within truly orthogonal orientations (Cribb and Scott, 1995; Kuwaba et al., 2001; Raspanti et al., 2002; Raspanti et al., 1997; Scott, 1988; Scott and Orford, 1981; Scott and Thomlinson, 1998; Van Kuppevelt et al., 1987). Use of homogenized orthogonal populations in molecular models may underestimate the amount of force transmitted across a given GAG bridge as function of the density of truly orthogonal GAGs. If each molecule deforms in exactly the same magnitude and direction, the load between neighboring fibrils would be distributed equally over the number of GAG linkages. While some molecules no doubt bridge the gap directly, others may be coaxial to the collagen or askew at some intermediate angle. Given an arbitrary deformation, certain molecules would be loaded immediately while others would be placed under compression.

Liao et al. measured GAG distributions in chordae tendineae using transmission electron microscopy (TEM) in an attempt to quantify changes in GAG orientation with applied tensile loading (Liao and Vesely, 2007). Unloaded samples showed GAG angles nearly orthogonal to the collagen axis and skewness increased with load, resulting in GAGs more coaxially aligned with the collagen. This study suggested a mechanical contribution of the GAGs in resisting deformation due to their apparent shift in orientation, yet the effect of GAG deformation due to spatial confinement in the ubiquitous ground substance was not evaluated. Liao did not explicitly address changes in shape of the molecules, but did note an apparent lengthening of GAGs under deformation. This supports the need for detailed spatial orientation information in molecular models since not all GAGs were lengthened identically, implying that GAG deformation is a function of initial orientation.

A limitation of the current study arises from the difference in perspective associated with TEM images of orthogonal planes. Fig. 4 shows a gross magnitude mismatch between the AP/ML distributions and the transverse distributions. GAGs cannot occupy the collagen volume and are therefore found between them. As viewed from the transverse plane there is significant overlap of GAGs into the viewing plane since GAGs are forced into the interfibrillar space. GAGs seen in the AP and ML planes are not as susceptible to this error since the collagen is relatively transparent and they are viewed along the length of the collagen. GAGs in the AP and ML planes are therefore less likely to be combined in overlap through the section thickness. As a result the transverse plane has a reduced number of detected GAGs as compared to the AP and ML planes.

Also, the reader must not attempt to quantify total tissue GAG content based on image GAG content. Detected GAGs are only fragments of longer GAGs that may span many measured images. No

attempt has been possible to correlate GAG length in a TEM section to assay quantifying GAG fragments since pre-processing renders samples viable for only one process or the other and TEM images are only a small fragment of a much larger TEM section. Unbiased stereology tells us estimation of global GAG content from extremely small experimental volumes is fraught with compounding errors that can significantly impact the confidence of the global estimate (Howard and Reed, 2004).

In conclusion, sulfated GAGs are distributed with transversely isotropic symmetry within the human MCL. The population has a majority of sulfated GAGs orthogonal to the collagen axis (70–90°), but up to half can be found at other angles with respect to collagen. The current data, along with the GAGSim3D model, can be used to generate probability densities of GAG distributions for future GAG mechanics models. The data can be discretized to more accurately interpret interfibrillar interactions by assigning properties based on the relative amount of GAGs at a given orientation under an applied deformation. This opens avenues to not only include GAG–GAG tensile bond contributions, but also compressive, permeability, space filling, and frictional contributions of the molecules. The new information will aid more thorough interpretation of roles of the GAGs in connective tissues.

#### Acknowledgment

Financial support from NIH #AR47369 is gratefully acknowledged.

#### References

- Amiel, D., Billings, E., Akeson, W., 1990. Ligament structure, chemistry, and physiology. In: Daniel, D. et al. (Eds.), *Knee Ligaments Structure, Function, Injury, and Repair*. Raven Press, New York, pp. 77–91.
- Amiel, D., Frank, C., Harwood, F., Fronck, J., Akeson, W., 1984. Tendons and ligaments: a morphological and biochemical comparison. *J. Orthop. Res.* 1, 257–265.
- Basalo, I.M., Raj, D., Krishnan, R., Chen, F.H., Hung, C.T., Ateshian, G.A., 2005. Effects of enzymatic degradation on the frictional response of articular cartilage in stress relaxation. *J. Biomech.* 38, 1343–1349.
- Basalo, I.M., Chahine, N.O., Kaplun, M., Chen, F.H., Hung, C.T., Ateshian, G.A., 2007. Chondroitin sulfate reduces the friction coefficient of articular cartilage. *J. Biomech.* 40, 1847–1854.
- Basalo, I.M., Mauck, R.L., Kelly, T.A., Nicoll, S.B., Chen, F.H., Hung, C.T., Ateshian, G.A., 2004. Cartilage interstitial fluid load support in unconfined compression following enzymatic digestion. *J. Biomech. Eng.* 126, 779–786.
- Chopra, R.K., Pearson, C.H., Pringle, G.A., Fackre, D.S., Scott, P.G., 1985. Dermatan sulphate is located on serine-4 of bovine skin proteodermatan sulphate. Demonstration that most molecules possess only one glycosaminoglycan chain and comparison of amino acid sequences around glycosylation sites in different proteoglycans. *Biochem. J.* 232, 277–279.
- Cribb, A.M., Scott, J.E., 1995. Tendon response to tensile stress: an ultrastructural investigation of collagen:proteoglycan interactions in stressed tendon. *J. Anat.* 187 (Pt 2), 423–428.
- Danielson, K.G., Baribault, H., Holmes, D.F., Graham, H., Kadler, K.E., Iozzo, R.V., 1997. Targeted disruption of decorin leads to abnormal collagen fibril morphology and skin fragility. *J. Cell Biol.* 136, 729–743.
- Duda, R.O., Hart, P.E., Stork, D.G., 2001. *Pattern Classification*, second ed. Wiley, New York.
- Ernst, S., Langer, R., Cooney, C.L., Sasisekharan, R., 1995. Enzymatic degradation of glycosaminoglycans. *Crit. Rev. Biochem. Mol. Biol.* 30, 387–444.
- Gardiner, J.C., Weiss, J.A., 2003. Subject-specific finite element analysis of the human medial collateral ligament during valgus knee loading. *J. Orthop. Res.* 21, 1098–1106.
- Gillard, G.C., Merrilees, M.J., Bell-Booth, P.G., Reilly, H.C., Flint, M.H., 1977. The proteoglycan content and the axial periodicity of collagen in tendon. *Biochem. J.* 163, 145–151.
- Goldoni, S., Owens, R.T., McQuillan, D.J., Shriver, Z., Sasisekharan, R., Birk, D.E., Campbell, S., Iozzo, R.V., 2004. Biologically active decorin is a monomer in solution. *J. Biol. Chem.* 279, 6606–6612.
- Haigh, M., Scott, J.E., 1986. A method of processing tissue sections for staining with cu-promeronic blue and other dyes, using CEC techniques, for light and electron microscopy. *Basic Appl. Histochem.* 30, 479–486.
- Henninger, H.B., Maas, S.A., Underwood, C.J., Whitaker, R.T., Weiss, J.A., 2007. Spatial distribution and orientation of dermatan sulfate in human medial collateral ligament. *J. Struct. Biol.* 158, 33–45.
- Howard, V., Reed, M.G., 2004. *Unbiased Stereology*, second ed. Garland Science/BIOS Scientific Publishers.

- Ilic, M.Z., Carter, P., Tyndall, A., Dudhia, J., Handley, C.J., 2005. Proteoglycans and catabolic products of proteoglycans present in ligament. *Biochem. J.* 385, 381–388.
- Iozzo, R.V., 1998. Matrix proteoglycans: from molecular design to cellular function. *Annu. Rev. Biochem.* 67, 609–652.
- Iozzo, R.V., 1999. The biology of the small leucine-rich proteoglycans. Functional network of interactive proteins. *J. Biol. Chem.* 274, 18843–18846.
- Kastelic, J., Galeski, A., Baer, E., 1978. The multicomposite structure of tendon. *Connect. Tissue Res.* 6, 11–23.
- Kuwaba, K., Kobayashi, M., Nomura, Y., Irie, S., Koyama, Y., 2001. Elongated dermatan sulphate in post-inflammatory healing skin distributes among collagen fibrils separated by enlarged interfibrillar gaps. *Biochem. J.* 358, 157–163.
- Liao, J., Vesely, I., 2007. Skewness angle of interfibrillar proteoglycans increases with applied load on mitral valve chordae tendineae. *J. Biomech.* 40, 390–398.
- Liu, X., Yeh, M.L., Lewis, J.L., Luo, Z.P., 2005. Direct measurement of the rupture force of single pair of decorin interactions. *Biochem. Biophys. Res. Commun.* 338, 1342–1345.
- Lujan, T.J., Underwood, C.J., Henninger, H.B., Thompson, B.M., Weiss, J.A., 2007. Effect of dermatan sulfate glycosaminoglycans on the quasi-static material properties of the human medial collateral ligament. *J. Orthop. Res.* 25, 894–903.
- Ottani, V., Raspanti, M., Ruggeri, A., 2001. Collagen structure and functional implications. *Micron* 32, 251–260.
- Pojasek, K., Shriver, Z., Kiley, P., Venkataraman, G., Sasisekharan, R., 2001. Recombinant expression, purification, and kinetic characterization of chondroitinase AC and chondroitinase B from *Flavobacterium heparinum*. *Biochem. Biophys. Res. Commun.* 286, 343–351.
- Pringle, G.A., Dodd, C.M., 1990. Immunoelectron microscopic localization of the core protein of decorin near the d and e bands of tendon collagen fibrils by use of monoclonal antibodies. *J. Histochem. Cytochem.* 38, 1405–1411.
- Quapp, K.M., Weiss, J.A., 1998. Material characterization of human medial collateral ligament. *J. Biomech. Eng.* 120, 757–763.
- Quinn, T.M., Dierickx, P., Grodzinsky, A.J., 2001. Glycosaminoglycan network geometry may contribute to anisotropic hydraulic permeability in cartilage under compression. *J. Biomech.* 34, 1483–1490.
- Raspanti, M., Congiu, T., Guizzardi, S., 2002. Structural aspects of the extracellular matrix of the tendon: an atomic force and scanning electron microscopy study. *Arch. Histol. Cytol.* 65, 37–43.
- Raspanti, M., Alessandrini, A., Ottani, V., Ruggeri, A., 1997. Direct visualization of collagen-bound proteoglycans by tapping-mode atomic force microscopy. *J. Struct. Biol.* 119, 118–122.
- Redaelli, A., Vesentini, S., Soncini, M., Vena, P., Mantero, S., Montevercchi, F.M., 2003. Possible role of decorin glycosaminoglycans in fibril to fibril force transfer in relative mature tendons—a computational study from molecular to microstructural level. *J. Biomech.* 36, 1555–1569.
- Robinson, P.S., Huang, T.F., Kazam, E., Iozzo, R.V., Birk, D.E., Soslowsky, L.J., 2005. Influence of decorin and biglycan on mechanical properties of multiple tendons in knockout mice. *J. Biomech. Eng.* 127, 181–185.
- Scott, J.E., 1985. Proteoglycan histochemistry—a valuable tool for connective tissue biochemists. *Coll. Relat. Res.* 5, 541–575.
- Scott, J.E., 1988. Proteoglycan–fibrillar collagen interactions. *Biochem. J.* 252, 313–323.
- Scott, J.E., 1992. Supramolecular organization of extracellular matrix glycosaminoglycans, in vitro and in the tissues. *FASEB J.* 6, 2639–2645.
- Scott, J.E., 1996. Proteodermatan and proteokeratan sulfate (decorin, lumican/fibromodulin) proteins are horseshoe shaped. Implications for their interactions with collagen. *Biochemistry* 35, 8795–8799.
- Scott, J.E., 2001. Structure and function in extracellular matrices depend on interactions between anionic glycosaminoglycans. *Pathol. Biol. (Paris)* 49, 284–289.
- Scott, J.E., 2003. Elasticity in extracellular matrix ‘shape modules’ of tendon, cartilage, etc. A sliding proteoglycan–filament model. *J. Physiol.* 553, 335–343.
- Scott, J.E., Orford, C.R., 1981. Dermatan sulphate-rich proteoglycan associates with rat tail-tendon collagen at the d band in the gap region. *Biochem. J.* 197, 213–216.
- Scott, J.E., Thomlinson, A.M., 1998. The structure of interfibrillar proteoglycan bridges (shape modules) in extracellular matrix of fibrous connective tissues and their stability in various chemical environments. *J. Anat.* 192 (Pt 3), 391–405.
- Scott, P.G., McEwan, P.A., Dodd, C.M., Bergmann, E.M., Bishop, P.N., Bella, J., 2004. Crystal structure of the dimeric protein core of decorin, the archetypal small leucine-rich repeat proteoglycan. *Proc. Natl. Acad. Sci. USA* 101, 15633–15638.
- Trowbridge, J.M., Gallo, R.L., 2002. Dermatan sulfate: new functions from an old glycosaminoglycan. *Glycobiology* 12, 117R–125R.
- Van Kuppevelt, T.H., Rutten, T.L., Kuyper, C.M., 1987. Ultrastructural localization of proteoglycans in tissue using cuproline blue according to the critical electrolyte concentration method: comparison with biochemical data from the literature. *Histochem. J.* 19, 520–526.
- Venkataraman, G., Sasisekharan, V., Cooney, C.L., Langer, R., Sasisekharan, R., 1994. A stereochemical approach to pyranose ring flexibility: its implications for the conformation of dermatan sulfate. *Proc. Natl. Acad. Sci. USA* 91, 6171–6175.
- Vesentini, S., Redaelli, A., Montevercchi, F.M., 2005. Estimation of the binding force of the collagen molecule–decorin core protein complex in collagen fibril. *J. Biomech.* 38, 433–443.
- Vogel, K.G., Paulsson, M., Heinegard, D., 1984. Specific inhibition of type I and type II collagen fibrillogenesis by the small proteoglycan of tendon. *Biochem. J.* 223, 587–597.
- Vogel, K.G., Ordog, A., Pogany, G., Olah, J., 1993. Proteoglycans in the compressed region of human tibialis posterior tendon and in ligaments. *J. Orthop. Res.* 11, 68–77.
- Weber, I.T., Harrison, R.W., Iozzo, R.V., 1996. Model structure of decorin and implications for collagen fibrillogenesis. *J. Biol. Chem.* 271, 31767–31770.
- Weiss, J.A., Gardiner, J.C., 2001. Computational modeling of ligament mechanics. *Crit. Rev. Biomed. Eng.* 29, 303–371.
- Weiss, J.A., Gardiner, J.C., Bonifasi-Lista, C., 2002. Ligament material behavior is nonlinear, viscoelastic and rate-independent under shear loading. *J. Biomech.* 35, 943–950.
- Yamamoto, E., Hayashi, K., Yamamoto, N., 2000. Effects of stress shielding on the transverse mechanical properties of rabbit patellar tendons. *J. Biomech. Eng.* 122, 608–614.